Quantum image control through polarization entanglement in parametric down-conversion

D. P. Caetano and P. H. Souto Ribeiro

Instituto de Física, Universidade Federal do Rio de Janeiro, Caixa Postal 68528, Rio de Janeiro, RJ 21 941972, Brazil

J. T. C. Pardal and A. Z. Khoury*

Instituto de Física, Universidade Federal Fluminense, BR-24210-340 Niteroi, RJ, Brazil

We demonstrate both theoretically and experimentally the manipulation of quantum entangled images, using the coupling between polarization entanglement and the entanglement for the transverse degrees of freedom. Starting from a two-crystal bright source of polarization-entangled photons, we arrive at a configuration in which we are able to prepare superposition states for the down-converted angular spectrum while the polarization superposition state is preserved. This scheme allows us to select the detected quantum image by performing projections onto polarization subspaces. We also demonstrate the potential of the system for applications to quantum cryptography of images.

I. INTRODUCTION

The increasing interest in quantum information processing and communication has given rise to the need for efficient sources of entangled states of a quantum system. In the optical domain, the production of polarization-entangled photon pairs in type-II parametric down-conversion [1] has allowed much progress in this matter. Among several applications, we may quote the demonstration of dense coding [2], teleportation [3], and entangled states of three photons [4]. More recently, a two-crystal geometry has been employed, yielding a bright source of polarization-entangled photons [5]. This source is composed of two adjacent down-conversion crystals cut for type-I phase matching. The photon pairs created by pumping these crystals are well described by a polarization-entangled quantum state of the kind $|HH\rangle + e^{i\phi}|VV\rangle$. The whole family of "Bell states" can be obtained by introducing wave plates in the signal and idler beams. The entangled state phase ϕ and the degree of polarization entanglement of the down-converted photon pairs can be varied by proper control of the pump beam polarization. As described in Ref. [5], the polarization entanglement is measured through polarization analysis of the down-converted photon pair. The coincidence counts exhibit interference fringes as a function of the analyzer angles, while the individual single counts on signal and idler beams are insensitive to polarization analysis. Fringe visibility depends on the degree of entanglement and on the detector's aperture.

The potential applications of such a source of entangled photons are unlimited and a different aspect of this setup was exploited in Ref. [6]. There, polarization entanglement was measured through position interference in a setup similar to the one used by Kwiat *et al* [5]. In Ref. [6], however, the two down-conversion crystals were placed about 1 cm apart from each other, giving rise to interference fringes in the coincidence-counting rate as one of the detectors was transversally scanned. A heuristic description was given for this

problem, based on a monomode theory. In this work, we present a multimode theory which describes how to control quantum images through polarization entanglement. Our treatment is based on the theory developed in Refs. [7,8], where it was shown that the spatial properties of the pump beam are transferred to the coincidence profile as a consequence of the phase-matching conditions in the crystal.

II. MULTIMODE QUANTUM STATE

We now derive the multimode quantum state generated by the two-crystal configuration taking into account the angular spectrum of the pump beam. See Fig. 1 as a reference. Both crystals will be considered as a box with dimensions L_x, L_y, and L_z. The crystals are labeled 1 and 2. Crystal 1 is centered at the origin of the coordinate system while crystal 2 is centered at $\mathbf{d} = d\hat{\mathbf{z}}$. We shall use first-order perturbation theory for parametric interaction assuming sufficiently weak pump power. The time evolution operator [7] is then of the form $U(t+\tau,t) = 1 + U_1^{(1)}(t+\tau,t,\mathbf{r}_1) + U_2^{(1)}(t'+\tau,t',\mathbf{r}_2)$, where τ is the interaction time, $\mathbf{r}$ is the position of the crystal's center, and $t' = t + d/c$. A pump beam provided by a collimated continuous-wave monochromatic laser can be treated under the paraxial aproximation, being described by a multimode coherent state $|v_{\epsilon_p}(\mathbf{q}_p)\rangle$, where $v_{\epsilon_p}(\mathbf{q}_p)$ is the angular spectrum, $\mathbf{q}_p$ is the transverse wave vector, and ϵ_p is the pump polarization vector. Furthermore, for a short $[(\mathbf{k}_s + \mathbf{k}_i - \mathbf{k}_p)_z L_z \ll 1)]$ and wide $[(\mathbf{k}_s + \mathbf{k}_i - \mathbf{k}_p)_j L_j \gg 1$, for $j = x, y]$ crystal the phase-matching condition is very restrictive only
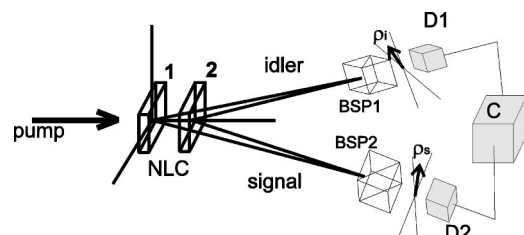

FIG. 1. Reference setup for theory.

---

*Corresponding author. Email address: khoury@if.uff.br

for the transverse components of the pump, signal, and idler wave vectors, imposing $\mathbf{q}_s + \mathbf{q}_i = \mathbf{q}_p$. Under these approximations, the first-order correction to the time evolution operator can be written [8] as

$$U^{(1)}(t+\tau,t,\mathbf{r}) = C \int d\mathbf{q}_s \int d\mathbf{q}_i e^{-i\phi(\mathbf{q}_s,\mathbf{q}_i,z)} v_{\epsilon_p}(\mathbf{q}_s + \mathbf{q}_i)$$
$$\times a_{\epsilon_s}^\dagger(\mathbf{q}_s) a_{\epsilon_i}^\dagger(\mathbf{q}_i) + \text{H.c.}, \quad (1)$$

where C is a constant, and $a^\dagger(\mathbf{q},\boldsymbol{\epsilon})$ and $a(\mathbf{q},\boldsymbol{\epsilon})$ are, respectively, the creation and annihilation operator of photons with transverse wave vector $\mathbf{q}$ and polarization $\boldsymbol{\epsilon}$.

As already mentioned, a short crystal does not impose a strict phase matching condition for propagation along z. This longitudinal phase-mismatch is accounted for through the function

$$\phi(\mathbf{q}_s,\mathbf{q}_i,z) = [\sqrt{k_s^2 - q_s^2} + \sqrt{k_i^2 - q_i^2} - \sqrt{k_p^2 - |\mathbf{q}_s + \mathbf{q}_i|^2}] z, \quad (2)$$

where z is the longitudinal coordinate of the crystal center. Therefore, $z_1 = 0$ and $z_2 = d$.

Now, let us consider the experimental situation found in Refs. [1] and [6]. The two crystals employed were cut for type-I phase matching with the optical axis rotated 90° with respect to each other. We shall suppose that the first crystal is oriented so that it is pumped by the vertical (V) polarization component, generating horizontally (H) polarized signal and idler photons. The second crystal is therefore pumped by the H polarization component, generating V polarized signal and idler photons. The down-converted modes are initially in the vacuum state, so that the quantum state generated by the parametric interaction up to first order is given by

$$|\psi\rangle = |\text{vac}\rangle + C \int d\mathbf{q}_s \int d\mathbf{q}_i v_V(\mathbf{q}_s + \mathbf{q}_i) |1_{\mathbf{q}_s,H} 1_{\mathbf{q}_i,H}\rangle$$
$$+ e^{-i\phi(\mathbf{q}_s,\mathbf{q}_i,d)} v_H(\mathbf{q}_s + \mathbf{q}_i) |1_{\mathbf{q}_s,V} 1_{\mathbf{q}_i,V}\rangle. \quad (3)$$

This quantum state will be used to obtain the transverse profile of the coincidence counts, giving rise to quantum images imprinted on the nonlocal two-photon correlations. Image-polarization entanglement arises from the polarization dependence of the pump angular spectrum in the quantum state above.

III. POLARIZATION-DEPENDENT QUANTUM IMAGES

We now turn to the coincidence profile at the detection planes, given by the normally ordered correlation function,

$$C(\mathbf{r}_s,\mathbf{r}_i) \propto \langle \psi | E^-(\mathbf{r}_s) E^-(\mathbf{r}_i) E^+(\mathbf{r}_i) E^+(\mathbf{r}_s) | \psi \rangle, \quad (4)$$

where $E^{+(-)}(\mathbf{r})$ is the positive (negative) frequency part of the electric-field operator at the detectors. When polarization analysis is performed before detection, through polarizing beam splitters (BSP), as in Refs. [1,6], for example, the detected field is decomposed as

$$E(\mathbf{r}_l) = E_H(\mathbf{r}_l)\sin\theta_l + E_V(\mathbf{r}_l)\cos\theta_l, \quad l=s,i, \quad (5)$$

where θ_l is the angle between the vertical axis and the transmission axis of the BSP placed in front of detector l. Contributions from modes entering the aparatus from the other port of each BSP will be disregarded. These modes are in the vacuum state and do not contribute to normally ordered correlation functions.

Coincidence detection is usually performed with interference filters that select the desired signal and idler wavelengths. For the degenerate case, $\omega_s = \omega_i = \omega_p/2$. These frequencies determine the detector positions according to the phase-matching conditions. For a monochromatic field, each polarization component ($\epsilon = H, V$) of the electric-field operator can be expanded as

$$E_\epsilon^+(\mathbf{r}_l) \propto \int d\mathbf{q}_l' a_\epsilon(\mathbf{q}_l') e^{i(\mathbf{q}_l' \cdot \boldsymbol{\rho}_l + \sqrt{k_l^2 - q_l'^2} r_{jl})}, \quad (6)$$

where $\boldsymbol{\rho}_l$ is the transverse position of detector l ($l=s,i$) and r_{jl} is the distance between the center of crystal j ($j=1,2$) and the origin of detection plane l. We recall that H polarized photons are created in crystal 1, while V polarized photons are created in crystal 2. These arguments lead to the following decomposition of the detected field operator:

$$E^+(\mathbf{r}_l) \propto \sin\theta_l \int d\mathbf{q}_l' a_H(\mathbf{q}_l') e^{i(\mathbf{q}_l' \cdot \boldsymbol{\rho}_l + \sqrt{k_l^2 - q_l'^2} r_{1l})}$$
$$+ \cos\theta_l \int d\mathbf{q}_l' a_V(\mathbf{q}_l') e^{i(\mathbf{q}_l' \cdot \boldsymbol{\rho}_l + \sqrt{k_l^2 - q_l'^2} r_{2l})}, \quad (7)$$

to be used in Eq. (4). From the whole family of 16 terms, there are only four nonvanishing contributions to the coincidence counting rate, namely, C_{HH}, C_{VV}, C_{HV}, and C_{VH}, where

$$C_{\epsilon\mu}(\mathbf{r}_s,\mathbf{r}_i) \propto \langle \psi | E_\epsilon^-(\mathbf{r}_s) E_\epsilon^-(\mathbf{r}_i) E_\mu^+(\mathbf{r}_i) E_\mu^+(\mathbf{r}_s) | \psi \rangle. \quad (8)$$

The total coincidence counting rate is therefore

$$C(\mathbf{r}_s,\mathbf{r}_i) \propto C_{HH}\sin^4\theta_A + C_{VV}\cos^4\theta_A$$
$$+ (C_{HV} + C_{VH})\sin^2\theta_A\cos^2\theta_A, \quad (9)$$

where we set $\theta_i = \theta_s = \theta_A$ for simplicity. The contributions $C_{\mu\epsilon}$ are more simply obtained by defining the kets $|\psi_\epsilon\rangle = E_\epsilon^+(\mathbf{r}_i) E_\epsilon^+(\mathbf{r}_s) | \psi\rangle$ so that $C_{\mu\epsilon} = \langle \psi_\mu | \psi_\epsilon \rangle$.

Let us assume for simplicity the degenerate cases $k_s = k_i = k$ and $k_p = 2k$, with a symmetric configuration such that the crystals are equidistant from signal and idler detectors $r_{1i} = r_{1s} = z$ and $r_{2i} = r_{2s} = z'$. For paraxial propagation ($q \ll k$) we have $\sqrt{k^2 - q^2} \approx k - q^2/2k$. The action of the electric-field operators on the quantum state $|\psi\rangle$ is readily performed by using

$$a_\mu(\mathbf{q}_l') |1_{\mathbf{q}_l,\epsilon}\rangle = \delta_{\mu\epsilon} \delta(\mathbf{q}_l - \mathbf{q}_l') |\text{vac}\rangle. \quad (10)$$

The vertical and horizontal components of the electric-field operator will have a relative phase due to the path difference from the crystals to each detector. This path difference will be taken into account by keeping only phase terms up to first order in $k(\mathbf{d} \cdot \boldsymbol{\rho})/z$, assuming $d \ll z$.

Therefore, a straightforward calculation leads to

$$|\psi_H\rangle = \frac{C}{4} e^{2ikz} \int d\mathbf{q}_+ v_V(\mathbf{q}_+) e^{i(\mathbf{q}_+ \cdot \boldsymbol{\rho}_+ - q_+^2 z/2k)}$$

$$\times \int d\mathbf{q}_- e^{i(\mathbf{q}_- \cdot \boldsymbol{\rho}_- - q_-^2 z/2k)} |\text{vac}\rangle \qquad (11)$$

and

$$|\psi_V\rangle = \frac{C}{4} e^{2ik(z - \mathbf{d} \cdot \boldsymbol{\rho}_+ /z)} \int d\mathbf{q}_+ v_H(\mathbf{q}_+) e^{i(\mathbf{q}_+ \cdot \boldsymbol{\rho}_+ - q_+^2 z/2k)}$$

$$\times \int d\mathbf{q}_- e^{i(\mathbf{q}_- \cdot \boldsymbol{\rho}_- - q_-^2 z/2k)} |\text{vac}\rangle, \qquad (12)$$

where we define the relative variables

$$\mathbf{q}_\pm = \mathbf{q}_i \pm \mathbf{q}_s \quad \text{and} \quad \boldsymbol{\rho}_\pm = \boldsymbol{\rho}_i \pm \boldsymbol{\rho}_s. \qquad (13)$$

In Eqs. (11) and (12) the integrals in $\mathbf{q}_+$ and $\mathbf{q}_-$ can be easily performed. The integrals in $\mathbf{q}_+$ are just the Fresnel integrals giving the pump field distribution $W_\epsilon(\boldsymbol{\rho}_+, z)$ for polarization ϵ at a distance z from the origin. The integrals in $\mathbf{q}_-$ give rise to phase factors which cancel out when coincidences are calculated. The resulting coincidence profile is therefore

$$C(\boldsymbol{\rho}_+) \propto \frac{|C|^2}{16} [\sin^4 \theta_A |W_V|^2 + \cos^4 \theta_A |W_H|^2$$

$$+ \sin^2 \theta_A \cos^2 \theta_A (W_V^* W_H e^{-i\varphi} + W_H^* W_V e^{i\varphi})]$$

$$= \frac{|C|^2}{16} |\sin^2 \theta_A W_V + \cos^2 \theta_A W_H e^{-i\varphi}|^2, \qquad (14)$$

where $\varphi = 2k\mathbf{d} \cdot \boldsymbol{\rho}_+ /z$. In the above expression the first two terms are the individual contributions of each crystal while the third term is the interference. The phase factor φ is responsible for the position interference measured in Ref. [6] and also has a direct effect on the fringe visibility for the polarization analysis performed in Ref. [1]. Indeed, integration over the finite aperture of the detectors will diminish the contribution of the interference term. In the experiments, $k \sim 10^7$ m^{-1}, $d \sim 10^{-2}$ m, and $z \sim 1$ m. Moreover, the angle between the down-converted beams and the pump beam is $\alpha \sim 0.12$ rad which means that φ performs about three cycles for each 1 mm variation of $\boldsymbol{\rho}_+$.

On the other hand, Eq. (14) shows that the spatial profile of the coincidence counts is a mixture of the images carried by the two polarization components of the pump beam. This is a consequence of the coupling between polarization entanglement and angular spectrum in the quantum state $|\psi\rangle$. An interesting application arises if the two orthogonal polarizations of the pump are rotated by an angle θ_P with respect to H and V. In this case the coincidence profile for two adjacent crystals ($\varphi = 0$) is

$$C(\boldsymbol{\rho}_+) \propto \frac{|C|^2}{16} |W_y (\cos^2 \theta_A \sin \theta_P + \sin^2 \theta_A \cos \theta_P)$$

$$+ W_x (\cos^2 \theta_A \cos \theta_P - \sin^2 \theta_A \sin \theta_P)|^2, \qquad (15)$$
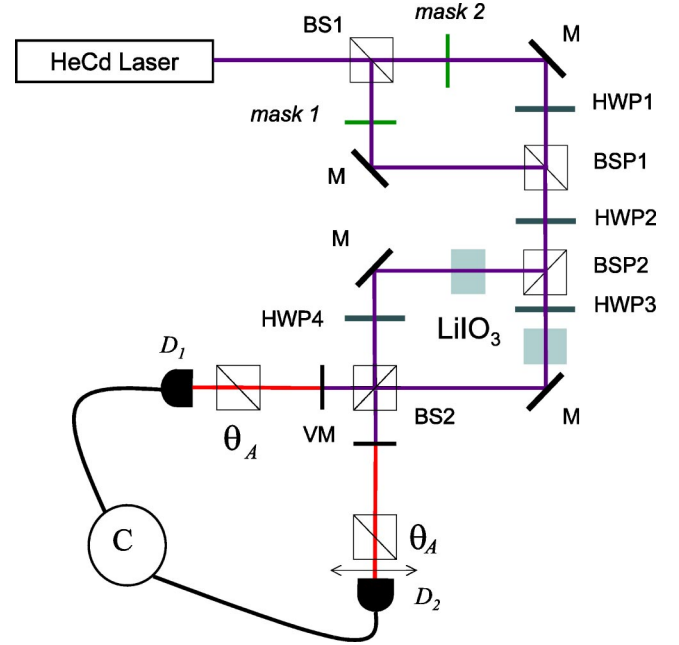

FIG. 2. Experimental setup. Collinear version.

where x and y are the two orthogonal polarizations of the pump. Therefore, an interesting application can be envisaged from Eq. (15). Let us suppose that W_y carries some information while W_x carries an enconding noisy image. From the result above, one can see that for a given θ_P there is always a suitable value of θ_A, which filters the information leaving the noisy contribution out of the coincidence profile. This suggests a scheme for cryptographic communication where the sender mixes the two images and sends the twin beams to a receiver who makes the polarization analysis. If the pump polarization is modulated by the sender, with an electro-optic device for example, there will be a suitable modulation of the analyzers for decoding the message.

IV. EXPERIMENT AND RESULTS

We have performed an experiment to demonstrate the manipulation of the image entanglement, acting on the polarization. Due to the phase-matching conditions of our crystals (two 1-cm-long LiIO$_3$ crystals cut for type-I phase matching) it was not possible to employ the two crystals in sequence as in Refs. [5] and [6]. We therefore built the experimental setup sketched in Fig. 2. The pump laser beam is divided in a 50/50 nonpolarizing beam splitter (BS1) and diffraction masks are placed in the beams of each output, so that they carry the angular spectrum corresponding to images of masks 1 and 2.

The polarization of the beam carrying image 2 is rotated 90° by a halfwave plate (HWP1) and the two images are recombined on a polarizing beam splitter (BSP1). Therefore, the pump beam carries two images in orthogonal polarization modes, a horizontal (H) and a vertical one (V). The vertical image is a collimated Gaussian and the horizontal image is a displaced focused Gaussian. Due to power limitations we were not able to employ more complicated profiles. In Fig. 3,
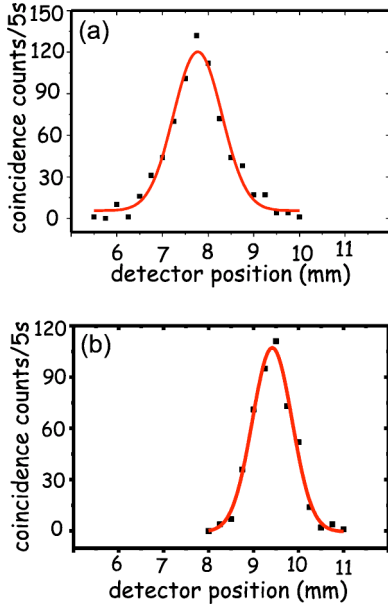
FIG. 3. (a) Image 1 transferred to both crystals (noise); (b) image 2 transferred to both crystals (information). $\theta_A = 45°$. Solid lines correspond to a Gaussian fit.

FIG. 4. (a) Information in the presence of noise ($\theta_P = 0°$ and $\theta_A = 45°$); (b) Recovered information ($\theta_P = -45°$ and $\theta_A = 45°$). Solid lines correspond to a Gaussian fit.

it is shown the coincidence counting rate when detector $D1$ is fixed and $D2$ is displaced along the horizontal transverse axis. In Fig. 3(a) the pump beam is blocked before mask 2 (image 1 transferred) and in Fig. 3(b) the pump beam is blocked before mask 1 (image 2 transferred). We shall call images 1 and 2 noise and information, respectively.

At the output of BSP1, we have placed a second half wave plate (HWP2) to produce a pair of orthogonal polarizations rotated by θ_P with respect to H and V. The second polarizing beam splitter (BSP2) then projects the modes carrying images 1 and 2 onto H and V polarizations, and distributes them between the two crystals. Instead of employing two crystals with orthogonal optical axis, we have oriented the optical axis of the two crystals parallel to each other and introduced a half wave plate (HWP3) before one of them. In order to achieve polarization entanglement, another half wave plate (HWP4) was introduced after the other crystal, so that signal and idler polarizations are rotated by 90°. Therefore, the V output of BSP2 pumps one crystal and generates a pair of H-polarized twin photons that are converted to V polarization by HWP4. The H output of BSP2 is converted to V by HWP3 and pumps the other crystal, generating a pair of H-polarized twin photons.

Under these conditions, the quantum state generated by the setup is

$$|\psi\rangle = |\text{vac}\rangle + C \int d\mathbf{q}_s \int d\mathbf{q}_i \, v_H(\mathbf{q}_s + \mathbf{q}_i)|1_{\mathbf{q}_s,H} 1_{\mathbf{q}_i,H}\rangle$$

$$+ e^{-i\phi(\mathbf{q}_s,\mathbf{q}_i,d)} v_V(\mathbf{q}_s + \mathbf{q}_i)|1_{\mathbf{q}_s,V} 1_{\mathbf{q}_i,V}\rangle. \quad (16)$$

Notice that this state is slightly different from the one given by Eq. (3), with respect to the polarization index. However,
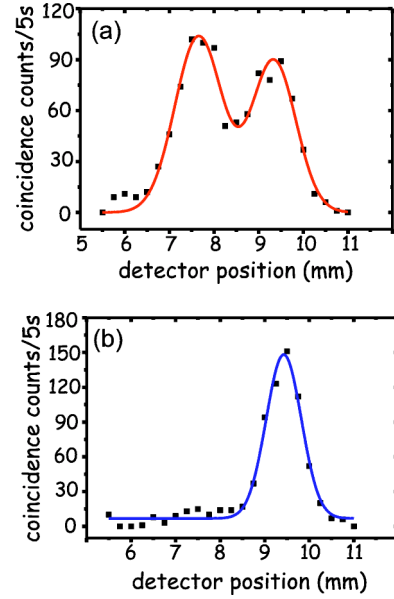
this difference is not important since the entanglement between polarization and transverse momentum degrees of freedom is still present.

Finally, the H-polarized and the V-polarized twin photons are mixed in a 50/50 nonpolarizing beam splitter (BS2). Each output of BS2 is filtered in order to block the transmitted pump beam and sent to a detector for coincidence detection. A polarizer is placed before each detector, both oriented at an angle θ_A with respect to V. A straightforward calculation on the same lines as the one leading to Eq. (15) gives the coincidence profile as
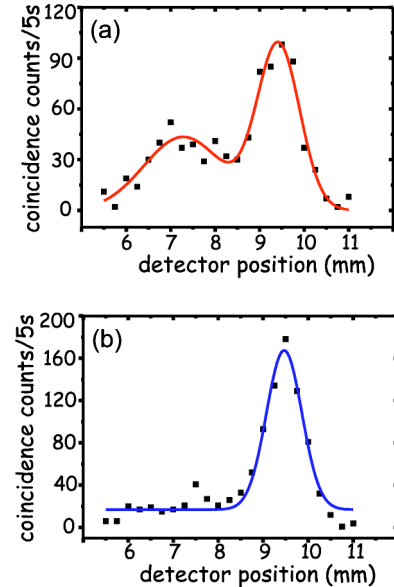

FIG. 5. (a) Information in the presence of noise ($\theta_P = -30°$ and $\theta_A = 45°$); (b) recovered information. $\theta_P = -30°$ and $\theta_A = 37°$. Solid lines correspond to a Gaussian fit.

$$C(\boldsymbol{\rho}_+) \propto \frac{|C|^2}{16} |W_y(\sin^2\theta_A \sin\theta_P + \cos^2\theta_A \cos\theta_P)$$
$$+ W_x(\sin^2\theta_A \cos\theta_P - \cos^2\theta_A \sin\theta_P)|^2, \quad (17)$$

where $W_x(\boldsymbol{\rho})$ and $W_y(\boldsymbol{\rho})$ are the two images carried by the pump beam, with polarizations x and y rotated by θ_P with respect to H and V. As before, for a given orientation of the pump (θ_P), there is an orientation of the analyzers (θ_A), which filters the noise and provides the cleaned information.

This principle is experimentally demonstrated in Figs. 4 and 5. In Fig. 4 the orientation of the analyzers is set to $\theta_A = 45°$. Figure 4(a) shows the noisy information obtained when the pump is oriented at $\theta_P = 0°$, while the cleaned information is recovered for $\theta_P = -45°$, as shown in Fig. 4(b).

In Fig. 5, θ_P is set to $-30°$ while the analyzers are varied to provide the noiseless information. In Fig. 5(a) the analyzers are oriented at $45°$ giving noisy information, while in Fig. 5(b) the noiseless information is recovered when the analyzers are set to $\theta_A = 37°$. All the above results are in agreement with the theoretical prediction given by Eq. (17).

V. CONCLUSION

We have applied a multimode theory for parametric down-conversion with two crystals. We have derived one expression for the coincidence-counting rate that takes into account the transfer of the angular spectrum of the pump beam in each crystal, the entanglement in polarization, and the effect of the coupling between these two degrees of freedom in the detection through polarization analyzers.

We have also adapted theory and experimental setup, starting from the two-crystal scheme, in order to demonstrate the manipulation of two quantum images performing projections onto polarization subspaces. Our results suggest that quantum cryptography can be further exploited with this system, as it is shown that the twin photons can be projected onto a subspace that mixes up or separates the two quantum images, depending on the polarization analyzing angles.

ACKNOWLEDGMENTS

[1] P. Kwiat *et al.*, Phys. Rev. Lett. **75**, 4337 (1995).

[2] K. Mattle *et al.*, Phys. Rev. Lett. **76**, 4656 (1996).

[3] D. Bouwmeester *et al.*, Nature (London) **390**, 575 (1997); D. Boschi *et al.*, Phys. Rev. Lett. **80**, 1121 (1998).

[4] D. Bouwmeester *et al.*, Phys. Rev. Lett. **82**, 1345 (1999).

[5] P. Kwiat *et al.*, Phys. Rev. A **60**, R773 (1999); A.G. White *et al.*, Phys. Rev. Lett. **83**, 3103 (1999).

[6] M. França Santos *et al.*, Phys. Rev. A **64**, 023804 (2001).

[7] Z.Y. Ou, L.J. Wang, and L. Mandel Phys. Rev. A **40**, 1428 (1989); L.J. Wang, Z.Y. Ou, and L. Mandel *ibid.* **44**, 4614 (1991); JOSA B **8**, 978 (1991).

[8] C.H. Monken *et al.*, Phys. Rev. A **57**, 3123 (1998); E.J.S. Fonseca *et al.*, *ibid.* **60**, 1530 (1999).